Pergamon

Int. J. Heat Mass Transfer. Vol. 39, No. 18, pp. 3949–3957, 1996

0017-9310/96 $15.00+0.00

0017-9310(95)00407-6

Numerical investigation of the interference effects between two burning fuel spheres

K. SIVASANKARAN, K. N. SEETHARAMU and R. NATARAJAN

Department of Mechanical Engineering, Indian Institute of Technology, Madras, India

(*Received* 1 *December* 1995)

Abstract—The interference effects between two burning spheres have been analyzed utilizing Labowsky's approach for problem formulation leading to the Laplace equation in a potential function and employing the finite-element method for its solution. The effect of separation on the interaction coefficient, the potential field and the flame geometry has been established. The critical spacing providing the demarcation between merged and separated flames is shown to be a function of the stoichiometric coefficient, radius ratio, ambient oxidizer concentration and ambient temperature. Correlations between the critical non-dimensional spacing and the critical interaction coefficient and the above parameters have been obtained for both equal- and unequal-sized drops. The cone criterion, originally proposed for equal drops, is extended to the case of unequal drops and the correlation between the cone half-angle and the parameters has been established. Copyright © 1996 Elsevier Science Ltd.

1. INTRODUCTION

In the recent past, considerable attention has been focused on the interference effects which occur when two fuel drops vaporize or burn in close proximity to each other [1–7]. The deviations from isolated single droplet vaporization or combustion behavior have implications for the modeling of spray diffusion flames. In all the above studies, the problem is reduced to the solution of the Laplace equation in the appropriate geometry. While Brzustowski *et al.* [3] and Umemura *et al.* [6, 7] have employed the bi-spherical co-ordinate system to solve the problem, Labowsky [1, 2, 4, 5] has utilized the modified images method for the solution. The former method is restricted to a system of two droplets, while the latter method may be extended to arrays of more droplets.

In the present work, the interference effects between two burning spheres have been analyzed utilizing Labowsky's approach for problem formulation, leading to the Laplace equation in a potential function and employing the finite-element method for solving it.

2. PROBLEM FORMULATION

With the standard set of assumptions employed in the literature for quasi-steady non-convective spherico-symmetrical droplet combustion, the combined fuel/oxidizer and temperature/oxidizer conservation equations reduce to the Shvab–Zeldovich form

$$\nabla\cdot[\rho v(Y_f - Y_o i_s) - \rho D\nabla(Y_f - Y_o - i_s)] = 0 \quad (1)$$

$$\nabla\cdot[\rho v(T + Y_o Q i_s/C_p) - \frac{k}{C_p}\nabla(T + Y_o Q i_s/C_p)] = 0. \quad (2)$$

The mass averaged velocity v may be expressed in terms of a velocity potential

$$v = -D\ln(1+B)\nabla\phi \quad (3)$$

where

$$\phi = \frac{-\ln[(1 - Y_f + Y_{o\infty} i_s)/(1 + Y_{i\infty} i_s)]}{\ln(1+B)}. \quad (4)$$

B is the transfer number for combustion

$$B = [C_p(T_\infty - T_1) + Q Y_{o\infty}/i_s]/L_v. \quad (5)$$

The steady-state mass conservation equation leads to the Laplace equation

$$\nabla^2\phi = 0 \quad (6)$$

subject to the following boundary condition:

$$\phi = \begin{cases} 1 & \text{on the droplet surface} \\ 0 & \text{far from the droplet.} \end{cases}$$

The introduction of the velocity potential ϕ has enabled the non-linear fuel/oxidizer conservation equation (1) to be reduced to the linear Laplace equation (6).

The interaction coefficient η is obtained as follows:

$$\dot{m} = \int\int \rho v \, ds \quad (7)$$

$$= \dot{m}_{iso}\eta \quad (8)$$

NOMENCLATURE

B	transfer number
C_p	specific heat of the gas phase
D	binary diffusion coefficient
d	drop diameter
i_s	stoichiometric coefficient ($= Y_{O,\infty}/Y_{F,s}$)
K	burning constant
k	thermal conductivity of the gas phase
L	non-dimensional separation; equal to s/d_s for unequal-sized drops
Q	heat of combustion
r	radius
rr	radius ratio
S	distance between the centers of drops
T	ambient temperature
T_s	drop surface temperature
v	mass-averaged velocity
Y_F	mass fraction of the fuel
$Y_{F,s}$	mass fraction of the fuel at the drop surface
Y_O	mass fraction of the oxidizer
$Y_{O,\infty}$	ambient oxidizer mass fraction.

Greek symbols

α	cone half-angle
ϕ	velocity potential
η	interaction coefficient $= m/m_{iso}$.

Subscripts

B	bigger drop
c	critical value
S	smaller drop
s	drop surface
∞	far from the drop
int	interacting drop
iso	isolated drop.

where $\dot{m}_{iso}$ is the burning rate of an isolated single droplet of the same size

$$\dot{m}_{iso} = 4\pi r\rho D \ln(1+B). \tag{9}$$

The dependent variable ϕ here replaces the dimensionless vapor density ρ^* for vaporizing spheres.

3. NUMERICAL SOLUTION PROCEDURE

Although the method of images employed by Labowsky may be applied to both symmetrical and unsymmetrical arrays, it appears to be cumbersome, while the bi-spherical coordinate system can only be applied to binary droplet systems, and a divergence problem is encountered. The finite element method offers a simpler, more direct and versatile method of solving the governing equation, which is linear, leading to convergent solutions.

By focusing attention on a binary sphere system, in the first instance, it is possible to reduce the problem to an axisymmetric one, with the axis passing through the centers of the spheres.

For this case the Laplace equation is

$$\frac{\partial^2\phi}{\partial r^2} + \frac{1}{r}\frac{\partial\phi}{\partial r} + \frac{\partial^2\phi}{\partial z^2} = 0 \tag{10}$$

which can be written as

$$\frac{1}{r}\left[\frac{\partial}{\partial r}\left(r\frac{\partial\phi}{\partial r}\right)\right] + \frac{\partial^2\phi}{\partial z^2} = 0 \tag{11}$$

with the same boundary condition ($\phi = 1$) on the circumference. The finite element mesh is constructed using axisymmetric triangular elements. Within each element, the ϕ distribution is related to the three nodal values by three interpolating functions $N_i(r, z)$ as follows

$$\phi = \sum_{i=1}^{3} N_i(r,z)\phi_i \tag{12}$$

where N_i, $i = 1, 2, 3$ are the shape functions and ϕ_i, $i = 1, 2, 3$ are the nodal values.

The shape function is given by

$$N_i(r,z) = \frac{1}{2A}(a_i + b_i r + c_i z) \tag{13}$$

where $a_i = r_j z_k - r_k z_j$; $b_i = z_j - z_k$; $c_i = r_k - r_j$ and A is the area of the element.

Galerkin's method is used to develop the finite element equations. It is basically a weighted residual method, where an approximate solution is substituted into the differential equation under consideration. Since the approximate solution does not satisfy the equation, a residual or error term R results. The Galerkin's method requires that

$$\int_V N_i R \, dV = 0. \tag{14}$$

The weighted residual integral for this case can be written as

$$\int_V [N]^T\left[\frac{1}{r}\frac{\partial}{\partial r}\left(r\frac{\partial\phi}{\partial r}\right) + \frac{\partial^2\phi}{\partial z^2}\right] dV = 0 \tag{15}$$

which results in a set of element equations of the form

$$[K]_{n\times n}\{\phi\}_{n\times 1} = \{f\}_{n\times 1} \tag{16}$$

where

$$[K] = \int r\left[\frac{\partial}{\partial r}[N]^{\mathrm{T}}\frac{\partial[N]}{\partial r} + \frac{\partial[N]^{\mathrm{T}}}{z}\frac{\partial[N]}{\partial z}\right]\mathrm{d}V \quad (17)$$

where

$$\mathrm{d}V = 2\pi r\,\mathrm{d}A \text{ and } \{f\} = 0.$$

The above set of element equations are solved after incorporating the boundary conditions.

A very fine mesh is taken in the region very close to the spheres. Both equal-sized and unequal-sized spheres have been investigated. The outer boundary is kept at 20 times the radius of the bigger sphere, since it is found that the location of the outer boundary does not affect the results when it is of the order of 20 r.

In order to calculate the interaction coefficient η, the derivatives of ϕ in the radial direction on the droplet are to be computed and integrated over the droplet surface. The derivatives are calculated by fitting a quadratic equation to the field variable ϕ as a function of the radial distance from the center of the concerned droplet

$$\phi(R) = a_0 + a_1 R + a_2 R^2. \quad (18)$$

4. RESULTS AND DISCUSSION

4.1. *Effect of separation on the interaction coefficient*

Theoretically, the interaction coefficient η is a function only of the dimensionless separation L and the radius ratio rr. Experimentally, Xiong *et al.* [8] have shown that η depends not only on the instantaneous geometry of the droplet assemblage characterized by the droplet sizes and separation distances, but also on the initial and aerothermochemical aspects of the system, such as the initial droplet sizes and separation distances, the fuel volatility and the transport properties.

The present results of η as a function of L show good agreement with those of Labowsky [4] and Umeumura *et al.* [7], with a maximum deviation of 4%. It is also seen that the approach to the isolated sphere value is smooth and continuous, and results have been obtained over a wider range of L.

Figure 1 shows the variation of η with the nondimensional spacing L for the four different values of radius ratio rr. When the spacing between the droplets is increased, η approaches the isolated sphere value of unity asymptotically. At a given separation distance, η for the smaller drop is less than that for the bigger drop. The curves for the smaller drops cross each other at L greater than 5. This occurs because for a fixed distance between the centers of the drops, when the radius of the smaller drop is decreased, the surfaces of the interacting drops recede from each other, thus causing a reduction in the interaction between the drops. In the case of equal-sized drops, the burning rate is minimum when the drops are touching each other, and monotonically increases as the spacing between the drops is increased, and approaches the isolated drop value of L greater than 10.

The following equations represent the variation of η with L for different rr, as shown in Fig. 1:

(a) $rr = 1 : \eta_{\mathrm{B}} = \eta_{\mathrm{S}} = 0.56 + 0.16L - 0.0022L^2 + 0.001L^3$ (19)

(b) $rr = 2 : \eta_{\mathrm{B}} = 0.84 + 0.05L - 0.006L^2 + 0.0003L^3$ (20)

$$\eta_{\mathrm{S}} = 0.25 + 0.50L - 0.15L^2 + 0.024L^3 - 0.002L^4 \quad (21)$$

(c) $rr = 4 : \eta_{\mathrm{B}} = 0.022\ln(L) + 0.945$ (22)

$$\eta_{\mathrm{S}} = 0.13 + 0.6L - 0.187L^2 + 0.03L^3 - 0.002L^4. \quad (23)$$

The subscripts B and S refer to bigger and smaller drops, respectively.

4.2. *Effect of separation on the ϕ-field*

Figure 2(a, b) shows the contour maps of ϕ for equal spheres at two different spacings. It can be seen that the gradient of ϕ in the region between the drops is decreased due to the interaction, and since the mass flux is proportional to the gradient of ϕ, there is a reduction in the burning rate. The ϕ field around each drop changes when the spacing is increased and tends towards that existing around an isolated drop.

A similar effect is observed in the case of drops of different sizes; the ϕ field is more distorted in this case. It is also found that the smaller drop is more affected by the interaction than the bigger drop. This can be ascribed to the fact that the ratio of the surface area facing the neighboring drop to its overall surface area is larger for the smaller drop. While calculating the ϕ gradient around the smaller drop, it has been found that at smaller spacing, the bigger drop's influence is felt not only on the side of the smaller droplet facing it, but also on the other side to a considerable extent. Hence, η for the smaller drop is a monotonically increasing function of spacing between the drops. While the burning rate of the bigger drop also decreases, the reduction is less than that for the smaller drop.

4.3. *Location of the flame surface*

The location of the quasi-steady flame surrounding the drops may be determined if it is assumed that the combustion rate is extremely rapid and the combustion reaction occurs at an infinitesimally thin zone. For this case, the flame region becomes a flame sheet. Setting $Y_{\mathrm{f}} = Y_{\mathrm{o}} = 0$ at the flame sheet, it follows from equation (4), that the quasi-steady flame will be located at

$$\phi = \phi_{\mathrm{F}} = \ln(1 + Y_{\mathrm{o}\infty} i_{\mathrm{s}})/\ln(1 + B). \quad (24)$$

This expression for the flame surface is similar to that obtained in quasi-steady single droplet com-

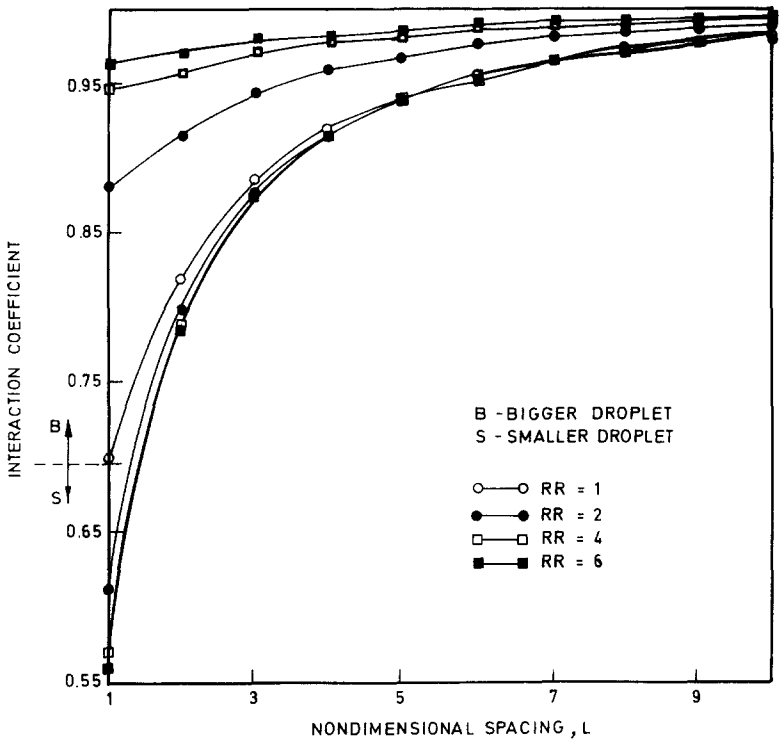

Fig. 1. Effect of inter-sphere separation on interaction coefficient for different radius ratios.

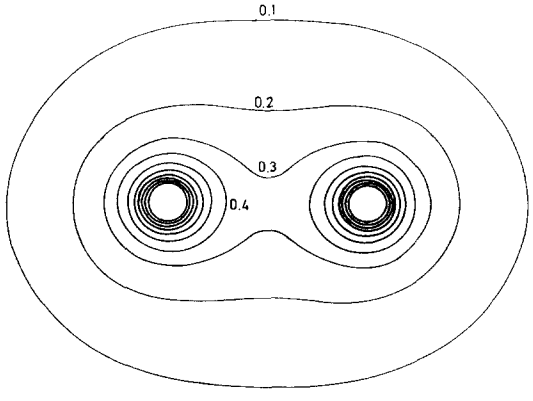

Fig. 2a. The ϕ field surrounding two interacting droplets; $rr = 1$; $L = 5$.

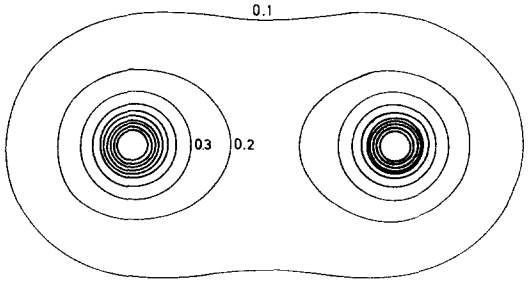

Fig. 2b. The ϕ field surrounding two interacting droplets; $rr = 1$; $L = 8$.

bustion theory, except that here the flame surface is not spherical, but is distorted by the interactions. In the region between the drop and the flame, only fuel vapour exists. This implies that the fuel is completely consumed at the flame surface, thus preventing it from reaching the ambience. The oxidizer is also completely consumed at the flame surface, thus preventing it from reaching the drop surface. Thus at the flame surface $Y_f = Y_o = 0$.

4.4. *Merged flames and separated flames*

These are two distinctly different types of flame surface, depending on the separation between the drops. When the drops are close together, a single flame surface encloses both the drops and appears in a more distorted form. On increasing the spacing between the drops, the flame eventually separates, and each drop is surrounded by an individual flame. These effects are shown in Fig. 3 for equal drops for a given combination of $Y_{o\infty}$ and T_∞. The critical separation distances are obtained from such series of figures for different combinations of rr, $Y_{o\infty}$ and T_∞.

It can be seen that the flame surfaces are more distorted on the side facing each other. This may be ascribed to the fact that the presence of the second drop prevents the penetration of the oxidizer towards the first drop. The presence of the neighboring drop brings in two effects: the first is to decrease the gradient of ϕ, and the second is to decrease the effective cross-sectional area through which the fuel and oxi-

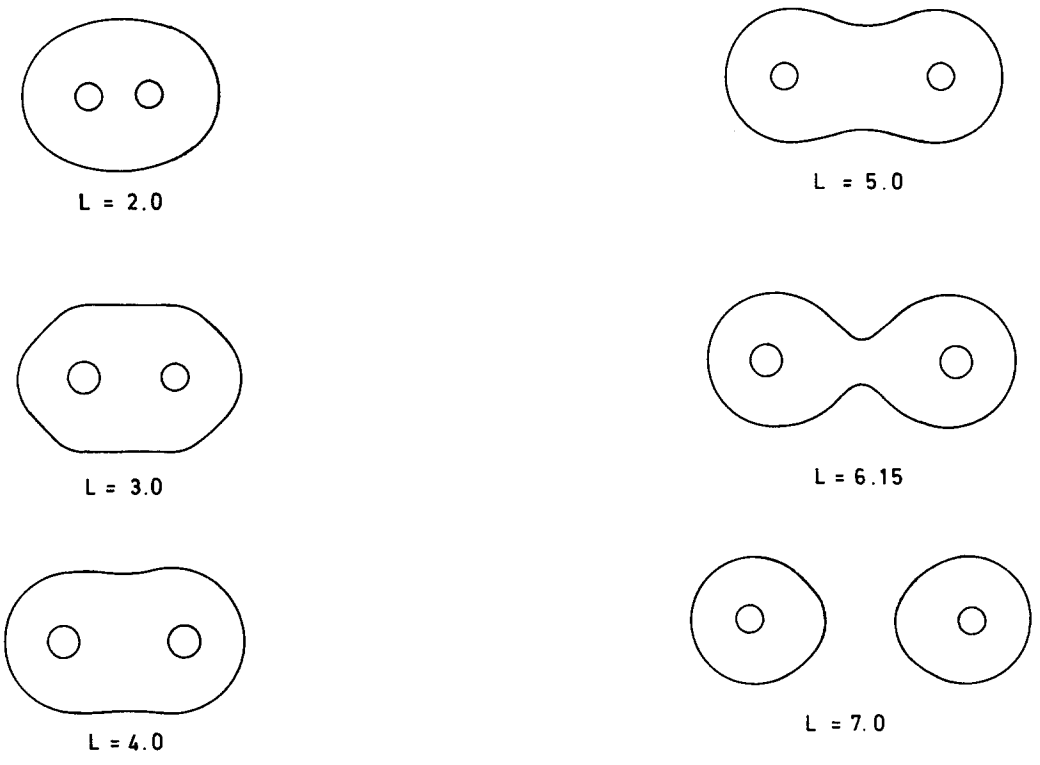

Fig. 3. Effect of L on flame shape $rr = Y_{oinf} = 0.2$, $T_{inf} = 15°C$, fuel: n-heptane.

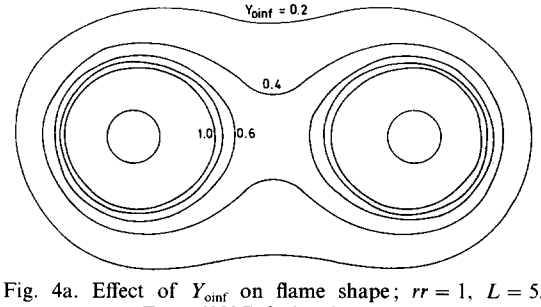

Fig. 4a. Effect of Y_{oinf} on flame shape; $rr = 1$, $L = 5$, $T_{inf} = 600°C$, fuel: n-heptane.

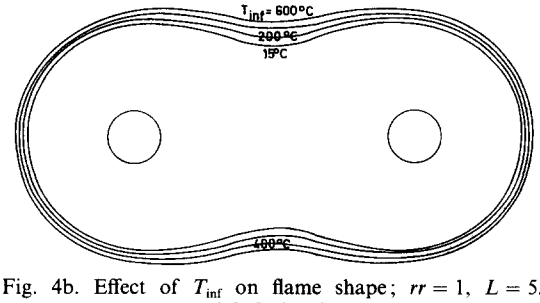

Fig. 4b. Effect of T_{inf} on flame shape; $rr = 1$, $L = 5$, $Y_{oinf} = 0.2$, fuel: n-heptane.

dizer are transported. The mass flux is proportional to both the gradient of ϕ and the effective cross-sectional area; hence the spherical symmetry characteristic of isolated drops is destroyed by the presence of a neighboring interacting drop. For large values of inter-drop spacing, the flames become more spherically symmetric around the individual drops. At these spacings, it is found that the burning rate of the interacting drops reaches 99.9% of the isolated drop value.

4.5. *The effects of ambient temperature and oxygen concentration on flame shapes*

The effects of T_∞ and $Y_{o\infty}$ have been investigated by noting the role they play in determining the value of ϕ_F in equation (24) and also through their influence on B, equation (5).

Figure 4(a) shows the effect of $Y_{o\infty}$ on flame shapes for equal drops at $L = 5$ and $T_\infty = 600°C$. Figure 4(b) shows the effect of T_∞ on the flame shapes for equal drops at $L = 5$ and $Y_{o\infty} = 0.2$; as T_∞ increases, the flame moves away from the drops. A change in T_∞ affects the transfer number B in the expression for ϕ_F. An increase in T_∞ increases B, which means that the driving force for mass transfer increases. Since this results in an augmentation of the diffusion of fuel vapor, the flame moves away from the drops. It is seen that the effect of $Y_{o\infty}$ is much stronger than that of T_∞ over the ranges of these parameters investigated. This is directly ascribable to their relative influence on ϕ_F and B: in the expression of ϕ_F, the effect of $Y_{o\infty}$ is more dominant than the effect of T, thus resulting in the behavior observed here.

Figure 5(a, b) shows the variation of B with $Y_{o\infty}$ and T_∞, and the consequent variation of ϕ_F with $Y_{o\infty}$ and T_∞. The transfer number B increases linearly with $Y_{o\infty}$; with increasing T_∞, B increases. ϕ_F increases

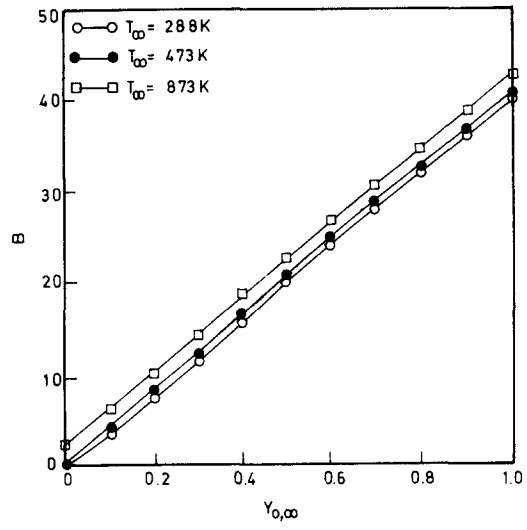

Fig. 5a. Variation of B vs $Y_{O,\infty}$.

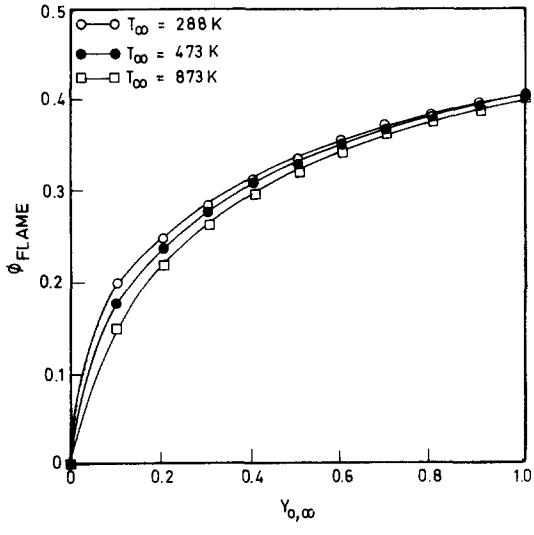

Fig. 5b. Variation of ϕ_{FLAME} vs $Y_{O,\infty}$.

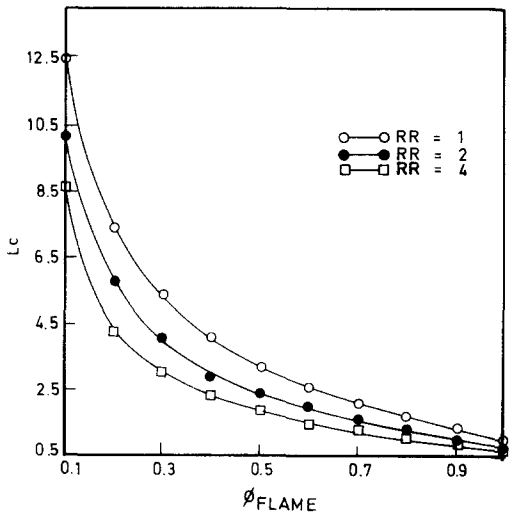

Fig. 6a. Effect of rr on the variation of Lc with ϕ_{FLAME}.

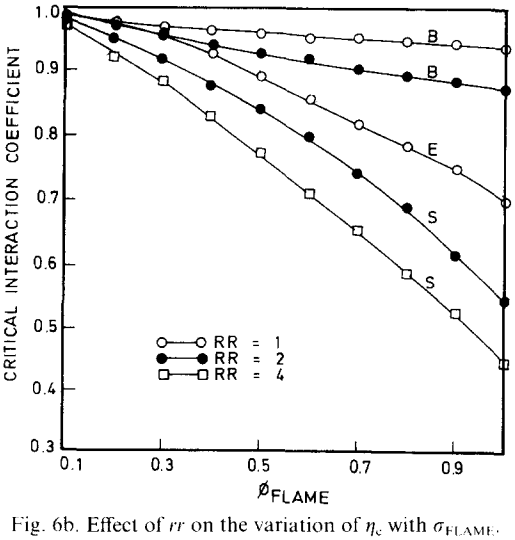

Fig. 6b. Effect of rr on the variation of η_c with σ_{FLAME}.

steeply with $Y_{O,\infty}$ upto $Y_{O,\infty} \approx 0.2$, and then the increase becomes less steep.

4.6. *The critical non-dimensional spacing* L_c

It is possible to define a critical non-dimensional spacing L_c at which a merged flame just separates into two flames, with increasing inter-drop separation. For a given value of radius ratio (rr), there exists a unique value of L_c for each value of ϕ_F. Figure 6(a) shows the effect of radius ratio on the variation of L_c with ϕ_F. It may be seen with reference to Fig. 2(a), for instance, that the contour corresponding to $\phi = 0.4$ has separated, but not at $\phi = 0.3$. Since ϕ has a value of 1 on the drop surface and zero far away from the drop, this shows that L increases as ϕ decreases; this also applies to the relationship between ϕ_F and L_c. Figure 6(a), together with equation (24), provides a criterion which determines the geometry of the flame. In Fig. 6(a), the region below the curves corresponds to merged flames, while the region above the curves corresponds to separated flames. The curves represent the locus of points corresponding to the critical spacing at which the two adjacent flames are just touching each other.

Figure 6(a) establishes the fact that the critical spacing is a function only of ϕ_F and rr. As far as the effect of rr is concerned, it is seen that at a given ϕ_F, L_c decreases with rr. An increase in the radius ratio decreases the interaction effect on the bigger drop. This brings the flame closer to the smaller drop.

For different fuel–oxidizer combinations, and temperature and oxygen concentration in the ambience, the critical separation may be obtained by first determining ϕ_F from equation (24), and then for the specified value of rr, referring to Fig. 6(a).

Figure 7(a) shows the effect of T_∞ on the variation of L_c with $Y_{O,\infty}$ for a value of $rr = 4$. It is seen that the effect of $Y_{O,\infty}$ is stronger than that of T_∞; this is true for the other two radius ratios also. An increase in the

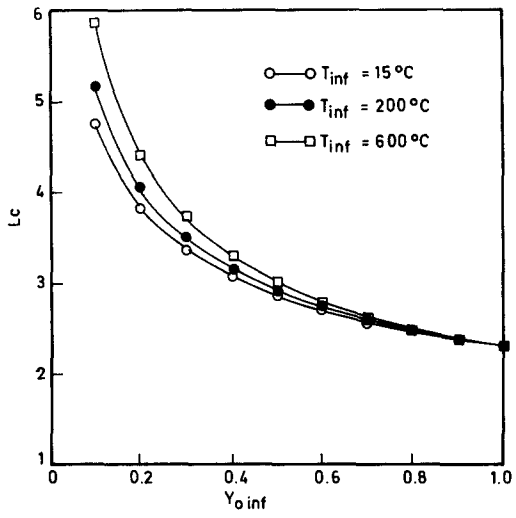

Fig. 7a. Effect of T_{inf} on the variation of Lc with Y_{oinf}; $rr = 4$, fuel: n-heptane.

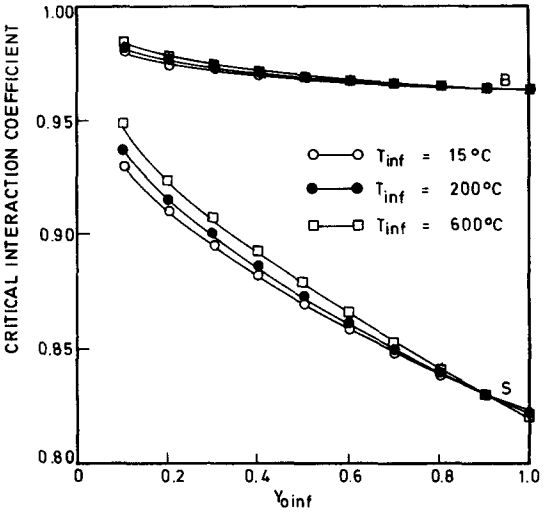

Fig. 8a. Effect of T_{inf} on the variation of η_c with Y_{oinf} for unequal droplets; $rr = 4$; fuel: n-heptane.

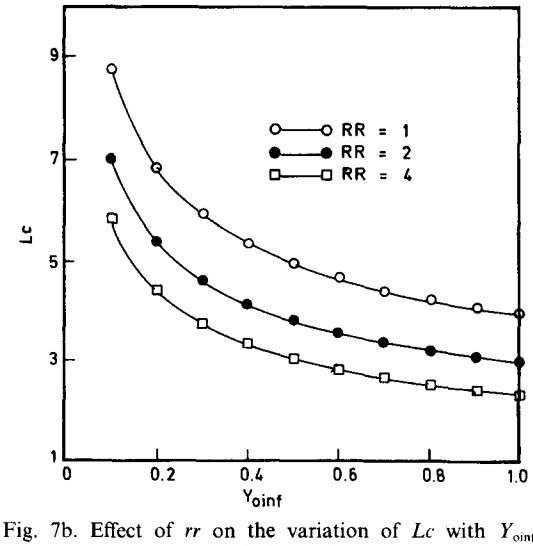

Fig. 7b. Effect of rr on the variation of Lc with Y_{oinf}; $T_{inf} = 600°C$, fuel: n-heptane.

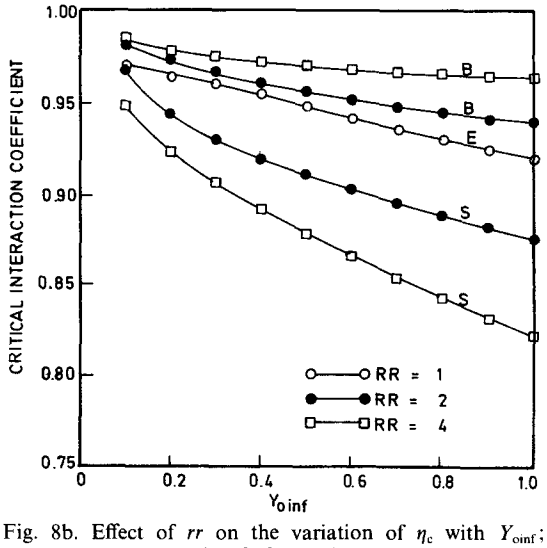

Fig. 8b. Effect of rr on the variation of η_c with Y_{oinf}; $T_{inf} = 600°C$, fuel: n-heptane.

radius ratio increases the gradient of the fuel vapor around the smaller drop, and thereby brings the flame closer to the smaller drop.

Figure 7(b) shows the effect of radius ratio on the variation of L_c with $Y_{o\infty}$ for $T_\infty = 600$ K. It is seen (by comparison with other values of T_∞) that the effect of $Y_{o\infty}$ is more dominant than that of T_∞; increasing rr causes a reduction in L_c.

4.7. *The critical interaction coefficient*

The critical interaction coefficient η_c may be defined as the value of η when the flames are exactly touching each other. While η is a function of rr and L_c, η_c is a function only of rr. The effect of rr on the variation of η_c and ϕ_F is shown in Fig. 6(b). The effect is qualitatively the same for different values of rr. An increase in ϕ_F decreases L_c, as shown in Fig. 6(a); η increases on increasing L, and hence η_c decreases when ϕ_F is increased.

Figure 8(a) shows the effect of T_∞ on the variation of the critical interaction coefficient η_c, for a value of $rr = 4$. As $Y_{o\infty}$ increases the interaction effect decreases and hence, η_c decreases. It is seen from the figure that the smaller drop (S) suffers more due to the interaction than the bigger drop (B).

Figure 8(b) shows the effect of radius ratio on the variation of η_c with $Y_{o\infty}$, for $T_\infty = 600$ K. This again shows the stronger influence of $Y_{o\infty}$ and rr than T_∞, and the greater interference effect suffered by the smaller drops in the case of unequal drop pairs.

4.8. *Correlations for* n-*heptane*

The correlations for L_c and η_c, for the case of n-heptane as fuel, are presented below

(a) *Critical non-dimensional spacing* L_c.

$$L_c = a_1 rr^b T_\infty^c - Y_{O\infty}^d \tag{25}$$

$$L_c = a_2 rr^b (T_\infty/298)^c (Y_{O\infty}/0.232)^d$$

$$a_1 = 2.72; \quad a_2 = 6.05$$

$$b = -0.35; \quad c = 0.05; \quad d = -0.34 \tag{26}$$

correlation coefficient = 0.996.

(b) *Critical interaction coefficient for the bigger drop*, η_{cB}.

$$\eta_{cB} = a_3 rr^e T_\infty^f Y_{O\infty}^g \tag{27}$$

$$\eta_{cB} = a_4 rr^e (T_\infty/298)^f (Y_{O\infty}/0.232)^g$$

$$a_3 = 0.92; \quad a_4 = 0.95$$

$$e = -0.02; \quad f = 0.002; \quad g = -0.016 \tag{28}$$

correlation coefficient = 0.707.

(c) *Critical interaction coefficient for the smaller drop* η_{cS}.

$$\eta_{cS} = a_5 rr^h T_\infty^i Y_{O\infty}^j \tag{29}$$

$$\eta_{cS} = a_6 rr^h (T_\infty/298)^i (Y_{O\infty}/0.232)^j$$

$$a_5 = 0.88; \quad a_6 = 0.97$$

$$h = -0.06; \quad i = 0.006; \quad j = -0.04 \tag{30}$$

correlation coefficient = 0.95.

It may be observed that the critical non-dimensional spacing, L_c is almost independent of T_∞; and the critical interaction coefficient, η_c is quite independent of rr, T_∞ and $Y_{O\infty}$, for both the bigger and the smaller spheres.

4.9. *The cone criterion for merged and separated flame*

Brzustowski *et al.* [3] have proposed a 'cone criterion' whereby two equal-sized drops burn with separated individual flames when they lie wholly within a cone whose half-angle depends only on stoichiometry. However, equation (24) shows that L_c depends not only on stoichiometry, but also on ambient conditions such as oxygen concentration and temperature. At the limiting condition, when the sphere is tangential to the cone, the cone half-angle is given by

$$\alpha = \arcsin(r/h) \tag{31}$$

(and not arc tan (r/h) as given in ref. [3]). Brzustowski *et al.* also indicated that their cone criterion might not be applicable to unequal spheres.

It is shown below that the cone criterion can be proposed in a form which is applicable for both equal and unequal drops. For unequal drops there are two cones, one for the bigger drop and another for the smaller drop. It can be shown that

$$\alpha_1 = \arcsin \frac{2rr}{r(2L_c+1)-1} \tag{32}$$

$$\alpha_2 = \arcsin \frac{2rr}{r(2L_c-1)+1}. \tag{33}$$

For equal drops, $rr = 1$, and

$$\alpha_1 = \alpha_2 = \arcsin(1/L_c). \tag{34}$$

While for equal drops the enveloping cone are symmetrical about the yy axis, for unequal drops they are unsymmetrical.

Figure 9(a) shows the enveloping cones for *n*-heptane as the fuel, for equal drops ($rr = 1$); $T_\infty = 15$°C and $Y_{O\infty} = 0.2$. For this case, $\alpha_1 = \alpha_2 = 9°16'$ (while in ref. [3] a value of 6.68° was obtained). The drops marked *A* burn together with a single flame, while those marked *B* burn with independent flames, and those marked *C* burn with flames which are just on the point of separation.

For unequal drops, with $rr = 2$, with the same ambient conditions as before, $\alpha_1 = 11°25'$ and $\alpha_2 = 6°18'$. These cones are shown in Fig. 9(b).

Figure 10 shows the variation of cone semi-angle α with ϕ_F for three different values of radius ratio. For any given fuel–oxidizer combination (fixing the stoichiometry), and for given ambient conditions of temperature and oxidizer concentration, ϕ_F is to be determined, from which the values of α for the bigger and smaller drops, or for equal drops, may be obtained from this figure.

Umemura *et al.* [6] have also proposed a criterion which determines the form of flame for equal drops, in terms of plots of $(Y_{O\infty} W_F v_F/W_O/v_O) = (Y_{O\infty}/i_S)$ vs ζ for four different values of $Y_{F,L}$. They propose that the region below the curves corresponds to merged flames, while the region above the curves corresponds to separated flames. For *n*-heptane with $Y_{O\infty} = 1$, $Y_{O\infty}/i_S = 0.285$, but the range given for the ordinate is from 0 to 20, with steep variations in the range from 0 to 3. In general, it can be shown that the maximum range in the y-axis applicable to the case of *n*-paraffins is from 0 to 1. For the *n*-paraffin represented by C_nH_{2n-2}, if M is the maximum value of the ordinate corresponding to $Y_{O\infty} = 1.0$, it can be shown that

$$\eta = \frac{1-8M}{24M-7}. \tag{35}$$

It is seen that for realistic values of n (such as 1, 2...), M has to be less than 1.

They have also presented three typical flame surfaces for benzene. They have taken $Y_{F,L} = 0.1$ for benzene, which is obviously too low a value. This leads to flame stand-off distances which are not realistic; the flame surface is located too close to the drop surface, which is not realistic, since even for the case of a single drop, the flame radius for hydrocarbon fuels is nearly 15 times the drop radius.

5. CONCLUSIONS

The Laplace equation in terms of the velocity potential based on the Shvab–Zeldovich formulation has been solved for a binary system of burning fuel spheres, employing the finite element technique. Results have been obtained for the interaction coefficient, the potential field and the flame geometry

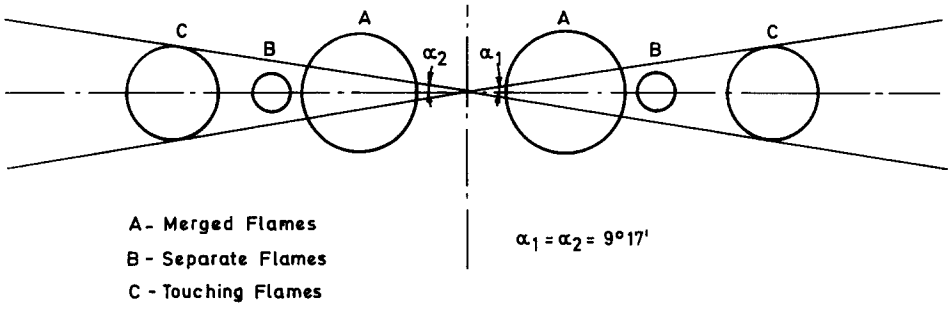

Fig. 9a. Enveloping cones; $rr = 1$, $T_{inf} = 15°C$, $Y_{oinf} = 0.2$, fuel: n-heptane.

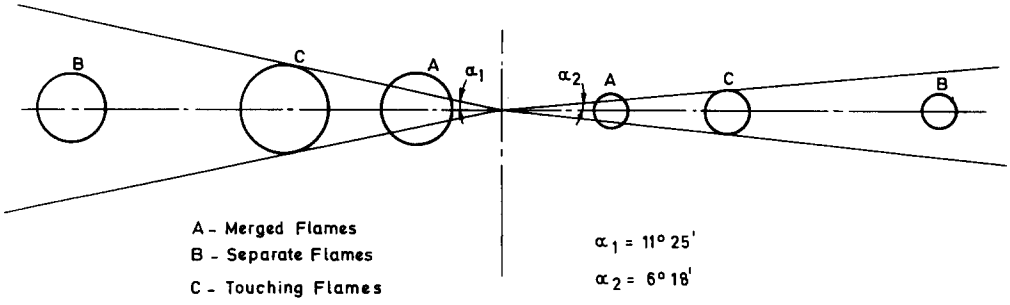

Fig. 9b. Enveloping cones; $rr = 2$, $T_{inf} = 15°C$, $Y_{oinf} = 0.2$, fuel: n-heptane.

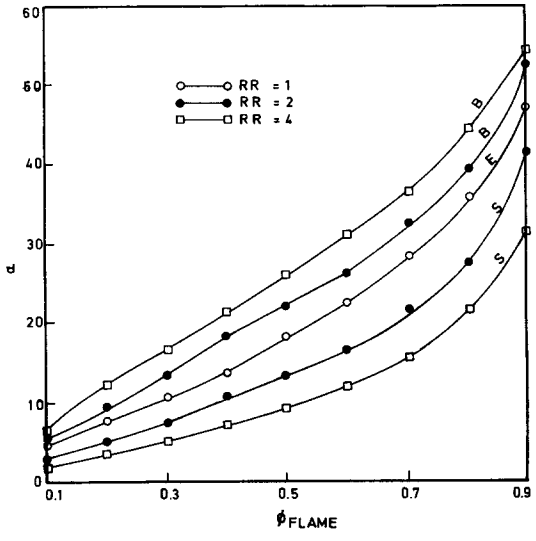

Fig 10. Effect of rr on the variation of α with ϕ_{FLAME}.

as a function of the inter-sphere separation. The critical spacing, which provides the demarcation between merged and separated flames, is shown to be a function of the stoichiometric coefficient, radius ratio, ambient temperature and ambient oxygen concentration. Correlations have been obtained, for both equal and unequal-sized drops, between the critical spacing and the critical interaction coefficient, and the above parameters. The cone criterion, which was originally proposed for equal drops, has been extended in this study to the case of two unequal drops; a correlation has been obtained between the cone half-angle and the relevant parameters.

REFERENCES

1. M. Labowsky, The effects of nearest neighbor interactions on the evaporation rate of cloud of particles, *Chem. Engng Sci.* **31,** 803–813 (1976).
2. M. Labowsky, A formalism for calculating the evaporation rates of rapidly evaporating particles, *Combust. Sci. Technol.* **18,** 145–151 (1978).
3. T. A. Brzustowski, E. M. Twardus, S. Wojcicki and A. Sobiesiak, Interaction of two burning fuel droplets of arbitrary size, *AIAA J.* **17,** 1234–1242 (1979).
4. M. Labowsky, Transfer rate calculations for compositionally dissimilar interacting particles, *Chem. Engng Sci.* **35,** 1041–1048 (1980).
5. M. Labowsky, Calculation of the burning rates of interacting fuel droplets, *Combust. Sci. Technol.* **22,** 217–226 (1980).
6. A. Umemura, S. Ogawa and N. Oshima, Analysis of the interaction between two burning droplets, *Combust. Flame* **41,** 45–55 (1981).
7. A. Umemura, S. Ogawa and N. Oshima, Analysis of the interaction between two burning fuel droplets with different sizes, *Combust. Flame* **43,** 111–119 (1981).
8. T. Y. Xiong, C. K. Law and K. Miyasaka, Interactive vaporization and combustion of binary droplet systems, *Twentieth International Symposium on Combustion*, The Combustion Institute, pp. 1781–1787 (1984).